PERGAMON

Vision Research 38 (1998) 2539–2549

Vision Research

Functional architecture of primate cone and rod axons

Andrew Hsu [a], Yoshihiko Tsukamoto [b], Robert G. Smith [a], Peter Sterling [a,*]

[a] *Department of Neuroscience, 123 Anatomy-Chemistry, University of Pennsylvania, Philadelphia, PA 19104-6058, USA*
[b] *Department of Biology, Hyogo College of Medicine, 663-8501, Japan*

Received 6 June 1997; received in revised form 29 September 1998

Abstract

The cone axon is nearly four times thicker than the rod axon (1.6 vs 0.45 μm diameter). To assess how signal transfer and integration at the terminal depend on cable dimensions, a transducer (cone = ohmic conductance, rod = current source) coupled via passive cable to a sphere with a chloride conductance (representing $GABA_A$ receptor) was modelled. For a small signal in peripheral cone with a short axon, steady photosignal transfers independently of axon diameter despite a significant chloride conductance at the cone terminal. Temporally varying photosignal also transfers independently of axon diameter up to 20 Hz and is attenuated only 20% at 50 Hz. Thus, to accomplish the basic electrical functions of a peripheral cone, a thin axon would suffice. For a foveal cone with a long axon steady photosignal transfers independently of axon diameter, but temporally varying photosignal is attenuated 5-fold at 50 Hz for a thick axon and 10-fold for a thin axon. This might contribute to the lower sensitivity of central retina to high temporal frequencies. The cone axon contains 14-fold more microtubules than the rod axon, and its terminal contains at least 20-fold more ribbon synapses than the rod's. Since ribbon synapses sustain high rates of exocytosis, the additional microtubules (which require a thicker axon) may be needed to support a greater flux of synaptic vesicle components.

Keywords: Retina; Photoreceptor axon; Compartmental model; Ribbon synapse; Transmitter release

1. Introduction

Phototransduction has been studied intensely [1,2], and so has transmission of the photosignal at the first synapse [3]. But the cable that connects the transducer to the synapse has been largely ignored even though the design might be complicated. There must be selective pressure to minimize axon diameter. For example, foveal cone axons form a thick mat (Henle's layer) on the optical path to the transducer, and these contribute to photon scatter and nonspecific absorption. Nevertheless, the cone axon is stout, about 1.6 μm in diameter.

The cone axon can be quite long (up to 500 μm in human fovea), so its large diameter might prevent spatial decrement of the photovoltage and also temporal filtering [4,5]. But even where the cone axon is short (20 μm), outside the fovea it is also thick. Conversely the rod axon, spanning a similar range of lengths, is always thin, about 0.45 μm in diameter. We wondered whether passive cable properties alone could explain this difference in caliber between cone and rod axons.

Possibly, additional factors influence cable design, such as the I–V relationship at the source and the load at the terminal. Such factors might also affect differently the steady voltage at the terminal and transfer of the photovoltage. To explore how such factors interact with cable dimensions, we constructed compartmental models of both cell types, capturing critical aspects of anatomical structure, I–V relations at the transducer, and alternative assumptions about the terminal load. We also noticed that the cone axon contains about 14-fold more microtubules than the rod; the ratio corresponding roughly to their difference in number of ribbon synapses. Since a ribbon synapse releases synaptic vesicles at high rates [6–11], a key constraint on axon diameter may be the number of microtubule 'tracks' needed for exchange of synaptic vesicle components with the soma.

* Corresponding author. Fax: +1 215 8989871; e-mail: peter@retina.anatomy.upenn.edu.

0042-6989/98/$19.00
PII: S0042-6989(97)00370-2

2. Methods

2.1. Structure

To measure axon dimensions, we studied retinal tissue from the fovea and near periphery (1 mm temporal) obtained from adult monkey (*Macaca fascicularis* and *M. fuscata*) fixed by perfusion with glutaraldehyde and paraformaldehyde. Retinal tissue was osmicated, stained with uranyl acetate, and embedded in Epon. Thin sections (1 μm) were cut along the horizontal and vertical meridians and stained with toluidine blue for light microscopy. Serial ultra-thin sections (0.09 μm thick) were cut radially along the horizontal meridian and photographed at 2000 × and 8000 × magnification in an electron microscope. The preparation of this tissue was described in detail elsewhere [12].

2.2. Function

Electrotonic properties were studied by compartmental modeling [13,14]. Computations used the NeuronC simulator [15] on a UNIX workstation. The photoreceptor model consisted of four elements: outer segment, inner segment, axon, and synaptic terminal (Fig. 1). Simulations generally assumed specific membrane resistance (R_m) = 50 kΩ cm^2 [16,17], cytoplasmic resistivity (R_i) = 200 Ω cm [5,18,17], and specific membrane capacitance (C_m) = 1 μF/cm^2 [19]. Simulations were also run with R_m = 25 and 100 kΩ cm^2.

2.2.1. Cone

The outer segment was modeled as a 1 nS conductance in series with an 8 mV battery and in parallel with a capacitor. The conductance and battery values agree with recordings from salamander cone that show a linear current-voltage relationship with a reversal potential of −8 mV [18] and with excised patch recordings of catfish cone outer segment that show linear (ohmic) cGMP-channels (Fig. 1; see Ref [20]). The capacitor value was estimated by calculating the surface area of the membranous infoldings (lamellae), about half of which appear continuous with the plasma membrane ([21] reviewed in Ref [22]). The surface of a lamella is $2\pi r^2$ and the total surface area in the outer segment is:

$$S = \frac{2\pi r^2 L}{2d} \quad (1)$$

where L is outer segment length and d is lamellar spacing (40 nm). The numerator is simply twice the outer segment volume. Outer segment volume is calculated to be 38 μm^3 for a foveal cone and 10 μm^3 for a peripheral cone [23,24]. Thus the outer segment capacitance is assumed to be 10.7 pF for a foveal cone and 2.4 pF for a peripheral cone.

The inner segment was a 1 nS conductance with a reversal potential of −60 mV in accord with primate recordings [25]. The cone inner segment contains voltage-sensitive conductances (salamander: [18,26]; primate: [25,27]). The cone inner segment contains voltage-gated conductances that would be activated over the normal resting voltage range. But these conductances can be considered linear for the small voltage changes evoked by low contrast stimuli. Under these circumstances such conductances can amplify the high frequency response of the membrane [28], but since they are localized to the inner segment, they would not directly affect transmission through the axon. Therefore we assumed ohmic conductances and restricted the model to 'small-signal analysis'.

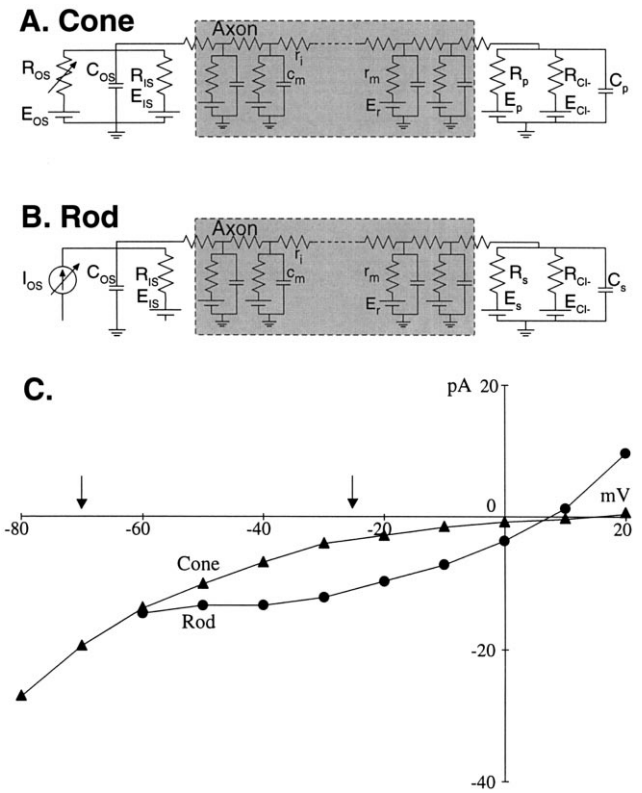

Fig. 1. (A) Compartmental model of the cone. Outer segment is a variable conductance (R_{OS}) in series with a battery (E_{OS}) and in parallel with a capacitor (C_{OS}); inner segment is another conductance (R_{IS}) in series with a battery (E_{IS}). See text for values. Axon is a cable (see Fig. 3(D)) subdivided into compartments 0.1 λ long. Terminal is a single compartment containing a conductance set by the terminal's dimensions and a battery (E_P) at −70 mV. An additional chloride conductance at the terminal up to 0.45 nS is simulated as an additional conductance (R_{Cl-}) plus battery (E_{Cl} −; −65 mV). For these parameters, the cone model consisted of ten compartments. (B) Compartmental model of the rod. Outer segment is a modulated current source (I_{OS}) in parallel with a capacitor (C_{OS}); inner segment is a conductance (R_{IS}) in series with a battery (E_{IS}; see text). Axon, terminal, and chloride conductances same as for cone. For these parameters, the rod model consisted of 17 compartments. (C) I–V relationship of cone and rod outer segment channels. Cone behaves as an ohmic conductance (rescaled from Ref [20]). Rod behaves as a current source (rescaled from Ref [2]). Arrows indicate approximate range of physiological voltages.

The cone axon was modeled as a cable of uniform diameter (1.6 μm). This cable matched results from a more detailed simulation of the anatomy (Fig. 3). The cone terminal was modeled as an isopotential sphere (7 μm diameter). With standard membrane parameters the model ranged from three compartments for the shortest axon (20 μm) to ten compartments for the longest (380 μm). Input impedance ranged from 0.5 GΩ for the cone with short axon to 0.4 GΩ in a cone with a long axon. Resting potential at the terminal ranged from −35 to −45 mV. These values of input resistance and resting potential accord with measurements from primate cones in situ [27] and also from salamander and turtle cones in isolation [5,18,29]. The model generated a dark current of about 30 pA, in agreement with measurements from macaque outer segments [24].

2.2.2. Rod

The outer segment was modeled as 35 pA current source in parallel with a 1.6 pF capacitor. The current source captured the rod's nearly flat $I–V$ relationship within the physiological range (Fig. 1[30,31]). The capacitance was calculated by assuming a cylindrical outer segment (25 μm long and 2 μm in diameter; [32]).

The inner segment's nonlinearities were avoided by restricting the model to a small light response (5% decrease in outer segment current), setting the current source in parallel with a 1 nS conductance and a leakage battery (−60 mV; [30,33]). The cable and sphere for rod axon and terminal were modeled like the cone's, differing only in the physical dimensions noted above. The rod model ranged from 3 compartments for a short axon (20 μm) to 17 compartments for a long one (380 μm). Input impedance ranged from 0.75 GΩ for a rod with short axon to 0.7 GΩ for a rod with long axon, and resting potentials ranged from −25 to −40 mV. These values of input resistance and resting potential accord with calculations/measurements for primate rod in situ [27] and from salamander rod in isolation [30,31,34,35].

2.2.3. Additional conductances

The mammalian cone terminal participates in a complex neural circuit which includes electrical coupling to neighboring terminals via gap junctions, voltage-sensitive Ca^{2+} channels, and negative feedback from horizontal cells (reviewed in Refs [36,37]). The gap junction conductance has a small driving force because adjacent cones tend to see the same stimulus. Although in fovea adjacent cones see somewhat different intensities at the highest spatial frequencies, contrast is so attenuated by the optics [38] that they tend to be isopotential. Therefore, the cone model omitted electrical coupling. Voltage-sensitive Ca^{2+} channels provide positive-feedback that would improve high frequency transmission across the synapse. Since this would tend to reduce the need for a thick cable, whose existence we sought to explain, we omitted these channels from the model.

Both cone and rod models considered horizontal cell feedback, which in primate is probably mediated by GABA [39,40]. Immunostaining for the $GABA_A$ Cl^- channel is associated with the photoreceptor synaptic complex [41] and, while $GABA_A$ has not yet been localized to the photoreceptor terminal itself, mRNA for the β subunit has been localized by in situ hybridization [42], and horizontal cell processes invaginating the rod terminal do form chemical synapses [43]. Consistent with this, a distinct inhibitory surround has been demonstrated by intracellular recordings from mammalian cone [44] and by indirect experiments [45]. Furthermore, GABA applied to the cone terminal in lower vertebrates modulates Cl^- channels ([46–48]; reviewed in Ref [49]). Peak Cl^- conductance might be expected in darkness when horizontal cell depolarization is maximal. The effects of such a chloride conductance were investigated by adding to the cone and rod terminal an additional leakage conductance of up to 0.45 nS (after Ref [29]), corresponding to about 25 $GABA_A$ channels [50]. The chloride reversal potential was assumed to be −65 mV [47].

3. Results

3.1. Structure

3.1.1. Foveal cone axons form a thick layer

Cone axons in the fovea (central 5°) pile up to form a defined layer, termed Henle's layer. This layer was up to 50 μm thick (Fig. 2A) and occupied 25–50% of the distance between the outer and inner limiting membranes (Fig. 2B). Thus, in the region serving highest acuity, Henle's layer contributes up to half of the retina's scattering and absorption (Fig. 2C) before photons are finally trapped at the inner segment waveguides immediately distal to Henle's layer [51,52].

3.1.2. Axon Dimensions

To find the actual length and taper of a foveal cone axon, we constructed seven of them from electron micrographs of serial sections (Fig. 3D). From soma to terminal, the axon extended 380 ± 5.5 μm (mean ± S.D.). This agrees with previous estimates of cone axon length in the fovea [53–56]. Emerging from the soma, the axon was 1.1 ± 0.2 μm in diameter, flaring to 1.4 ± 0.1 μm, and then 1.8 ± 0.2 μm, and finally tapering to 1.1 ± 0.1 μm just before the cone pedicle (Fig. 2B, arrows). Aside from the relatively short tapered segments at either end, thickness remained fairly constant over the proximal half (1.4 μm) and over the distal half (1.8 μm). Cross-sections through the cone

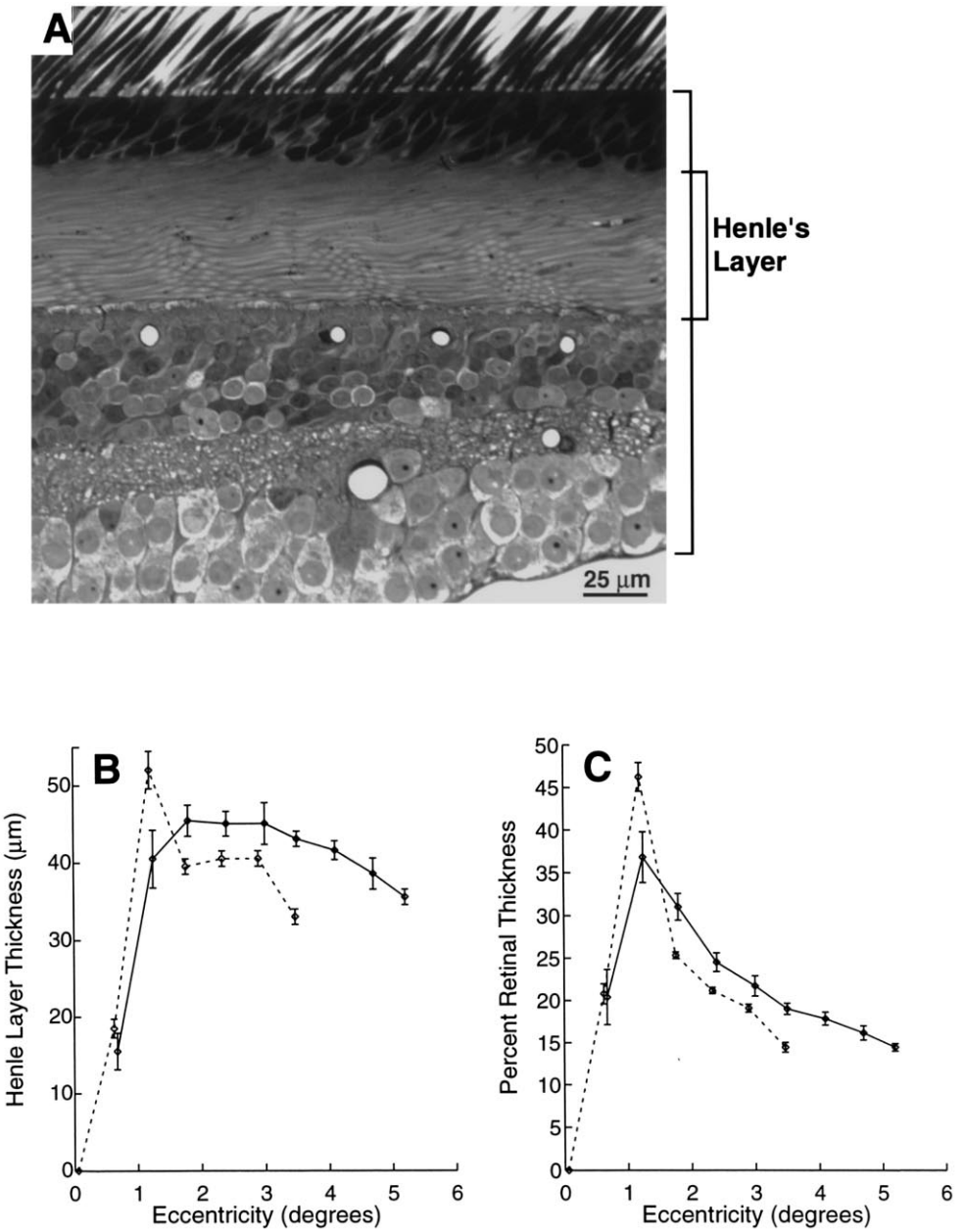

Fig. 2. (A) Radial section through fovea. Note thick layer of Henle. (Light micrograph, *M. fasicularis*). (B) Thickness of Henle layer shifts with eccentricity. Measurements were made along the horizontal (–) and vertical meridians (– – –). Error bars indicate S.D. (C) Henle's layer contributes a large fraction of the total postreceptoral thickness. Postreceptoral thickness is the distance from the cone outer limiting membrane through the ganglion cell axon layer. Symbols same as in (B).

axon in *M. fuscata* measured 1.55 ± 0.13 μm. The cone terminal was approximately rectangular, $4 \times 5 \times 7$ μm.

Rod axons in the perifovea of *M. fasicularis* were 0.45 μm diameter (Fig. 3A, B) and in *M. fuscata* 0.42 ± 0.03 μm. The axons were not traced, but Golgi studies at this eccentricity show them to be as long as foveal cone axons [53]. The rod axon terminal was spheroidal, about 2 μm in diameter.

3.1.3. Microtubules

Noting that cone and rod axons are filled with evenly spaced microtubules, we measured their distributions (Fig. 3B, C). A foveal cone axon in cross-section contained 440 ± 15 tubules at a density of $239 \pm 36/\mu m^2$ (Fig. 3(B)). A perifoveal rod axon contained 35 ± 4 at a density of $265 \pm 26/\mu m^2$. The mean densities were the same ($P > 0.8$), so the ratio of microtubules in the cone and rod axon is the same as the ratio of their cross-sectional areas, ~ 14.

3.2. Function

3.2.1. Steady (DC) photovoltage at the cone terminal

To investigate how cone axon dimensions affect transfer of the steady state response, we simulated a small photosignal as a 5% decrease in outer segment conductance. For a short axon, photovoltage at the terminal is insensitive to axon diameter (Fig. 4A). A chloride conductance at the terminal (0.45 nS) drastically reduces photovoltage for an axon thinner than 0.5 μm, but affects photovoltage little for axons thicker than this (Fig. 4A). For a long axon photovoltage is slightly attenuated below 0.5 μm diameter, but above this photovoltage is independent of axon caliber (Fig. 4B). A chloride conductance at the terminal attenuates photovoltage for thinner axons, and even for the true diameter (1.6 μm) a leak reduces photovoltage by 25%. These observations hold for R_m between 25 and 100 kΩ cm^2. Apparently the standard (short) cone axon needs to be at least 0.5 μm thick to allow sizeable photovoltages in the presence of a terminal chloride leak, but beyond 0.5 μm, there is no advantage. However, for the special case (long axon), increasing diameter beyond 0.5 μm improves photovoltage, particularly if there is a chloride leak.

3.2.2. Static photovoltage at the rod terminal

To investigate how rod axon dimensions affect transfer of steady state response, a small photosignal was simulated as a 5% decrease in the outer segment current. For a short axon photovoltage at the rod terminal is insensitive to axon diameter (Fig. 4A). But a chloride leak at the terminal reduces photovoltage greatly, and still more so for diameters below 0.5 μm. For a long axon, photovoltage is similar to the short axon at the true diameter (near 0.5 μm), but declines with increasing diameter (Fig. 4B). This decline in photovoltage with increasing diameter is due to an impedance mismatch between the current source transducer and the axon + terminal. A leak at the terminal greatly reduces photovoltage (Fig. 4B). Apparently the rod axon at its true diameter is thick enough to transfer the maximum photovoltage for both short and long axons, but in both cases a terminal leak greatly attenuates the signal.

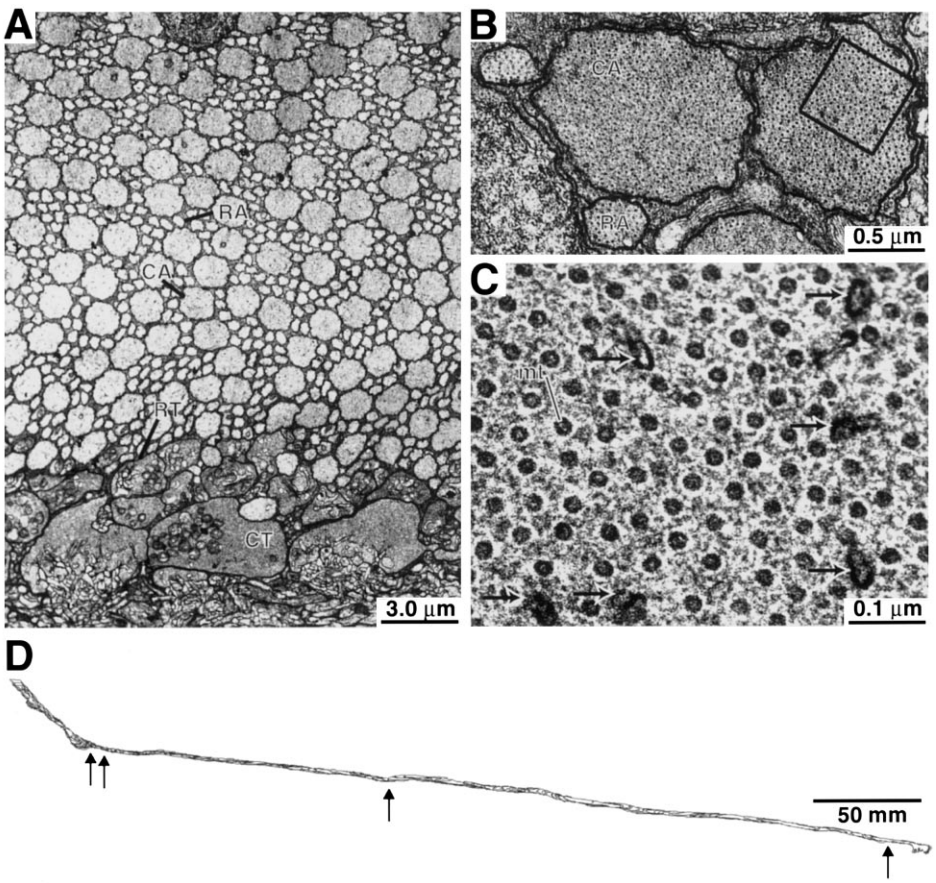

Fig. 3. (A). Radial section through Henle's layer in perifovea. (Electron micrograph, M fuscata). Cone axons (CA) are 4-fold thicker than rod axons (RA). Cone terminals (CT) are also much larger than rod terminals (RT). (B) Cone and rod axons are filled with microtubules. Square indicates region enlarged in C. (C) Microtubules (mt) in cone axon are evenly spaced and associated with patches of smooth membrane (arrows). (D) Foveal cone reconstructed from electron micrographs of serial sections. (*M. fasicularis*; inner segment at 1.45° nasal). Arrows indicate changes in axon diameter.

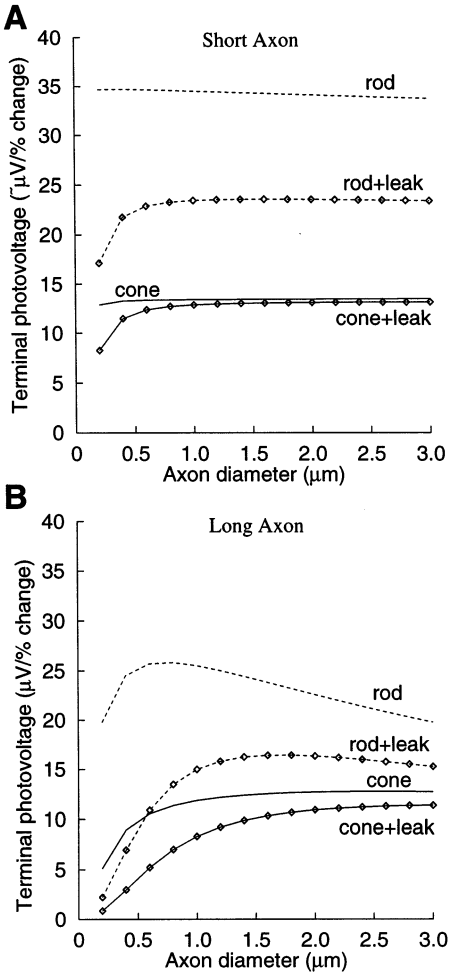

Fig. 4. Photovoltage at the terminal is independent of axon diameter. (A) Short axon (20 μm). Terminal photovoltage is greater for rod than cone. Load at terminal affects photovoltage at small axon diameters for rod but not for cone. For neither cell does photovoltage improve for axon diameters greater than about 0.5 μm. (B) Long axon (380 μm). Same computations as in A. Photovoltage does not improve with axon diameter above about 0.75 μm.

3.2.3. Resting voltage at cone terminal

For a cone axon of true diameter (1.6 μm) a large Cl^- leak at the terminal hardly affects the photovoltage (Fig. 5A). The leak has no effect because photovoltage is determined mainly by the outer and inner segment conductances. However, the leak does sharply hyperpolarize the terminal's steady potential (Fig. 5B). This is because leakage is the major conductance at the terminal and thus shifts the terminal's steady potential toward the chloride reversal potential (-65 mV). Thus, a GABA-mediated leak could strongly alter a terminal's steady potential while minimally affecting the photovoltage. An additional contribution to this leak could be caused by the Cl^- current accompanying glutamate transport [57,58].

3.2.4. Resting voltage at rod terminal

For a rod axon of true diameter (0.45 μm), any added leak strongly attenuates photovoltage at the terminal (Fig. 5A). This is true for both short and long axons. Because of the current source transducer, leakage is a major determinant of photovoltage at the terminal. Steady potential is also sharply hyperpolarized (Fig. 5B). Like the cone, leakage is the major conductance at the terminal so it shifts the terminal steady potential toward its reversal potential (-65 mV).

3.2.5. Propagation velocity

We calculated propagation velocity for a long rod and a long cone axon by simulating a voltage impulse at the outer segment and then measuring the time to peak response at the synaptic terminal. The cone signal propagates at about 150 μm/ms, and the rod signal at

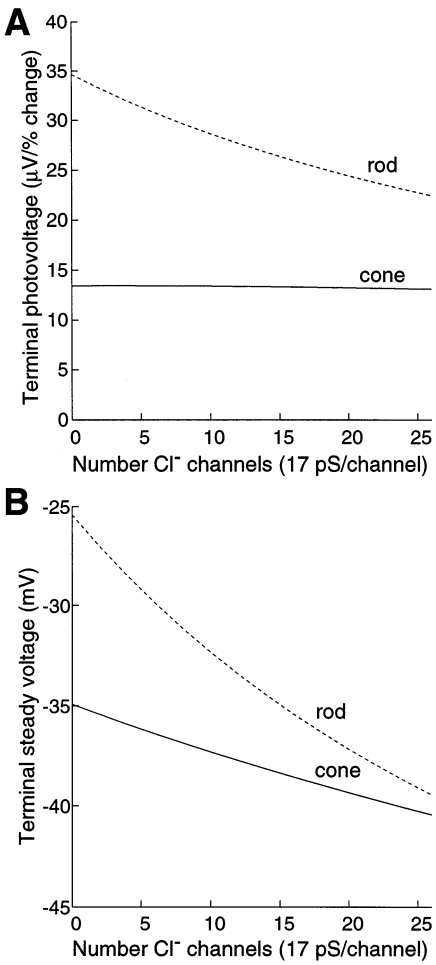

Fig. 5. Chloride leak at the terminal affects rod and cone signaling differently. (A) Terminal photovoltage vs leak for standard length (short) axons. Increasing leak in rod terminal attentuates photovoltage up to 30%, but leak in cone terminal has no effect. (B) Terminal steady potential vs leak for standard length (short) axons. Increasing leak hyperpolarizes the rod terminal strongly but the cone terminal only weakly.

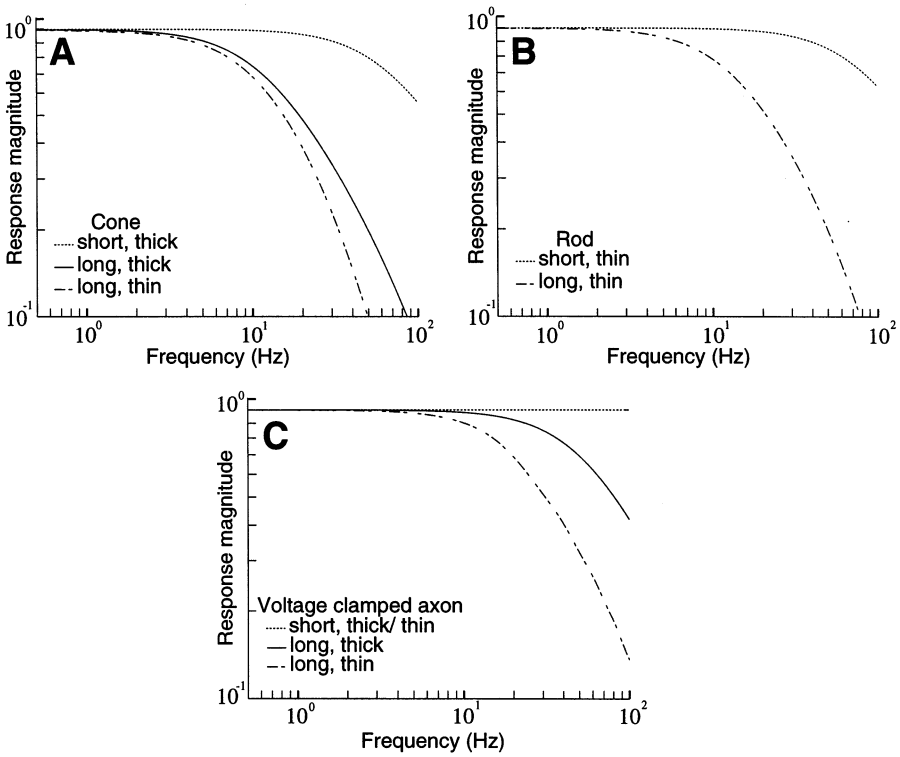

Fig. 6. Temporal response at terminal is determined by the transducer properties as well as the axon dimensions. (A) Cone terminal. Voltage response to an impulse conductance change at the outer segment. (B) Rod terminal. Voltage response to an impulse current change at the outer segment. (C) Voltage response at the photoreceptor terminal to a voltage clamped impulse at the outer segment. Response is flat for a short axon. Response declines at about 20 Hz in a long, thin axon and at about 30 Hz for a long, thick axon. But even at 100 Hz, neither axon attenuates by more than one log unit.

about 75 μm/ms. The cone photosignal reaches the terminal in about 2.5 ms while the rod photosignal requires 5 ms. This difference is likely explained by the 4-fold difference in axon diameter since propagation velocity is proportional to the square root of the diameter [19].

3.2.6. Temporally varying photosignal

Peripheral cone outer segments respond to bright flashes with considerable power up to 40–50 Hz [24,27], so it we computed how axon dimensions might affect transfer of a temporally varying signal. Simulating an impulse in outer segment conductance (cone) or current (rod), we measured the terminal's response, and then obtained the Fourier transform. For the peripheral cone (short axon), the signal transfered independently of axon diameter up to 20 Hz and was attenuated by only 20% at 50 Hz (Fig. 6A). For the foveal cone (long axon) attenuation at 50 Hz was 5-fold for a thick axon and 10-fold for a thin axon (Fig. 6A).

For the rod axon of true diameter (0.45 μm), both short and long axons gave flat frequency responses up to 10 Hz (Fig. 6B). Attenuation was stronger for the long axon at higher frequencies. Responses of rod outer segments to short, dim flashes contain most of their power in the range 1–5 Hz [27,32]. Since the true rod axon dimensions show minimal decrement in this range (Fig. 6B), the rod axon does not limit the transfer of small rod signals.

To isolate the contribution of the axon and terminal to the temporal response, a voltage was applied at impulse at the outer segment and computed the frequency response was computed (Fig. 6C). For short axons, frequency response was flat well past 100 Hz. For long axons, thick was better since there was less axial resistance. However, even a long, thin axon offered a surprisingly good response (i.e. no decrement at 10 Hz and little at 20 Hz). A comparison of the response to voltage clamp (Fig. 6C) with the response to conductance/current impulse (Fig. 6A, B) suggests that photoreceptor temporal responses depend on the outer segment membrane properties as well as on the axon.

4. Discussion

The usual concern regarding signal transfer down a passive cable is the spatial decrement of voltage and temporal filtering. Thus it has been suggested that photovoltage might be markedly attenuated by the axon of a foveal cone [5] and a rod [59]. However,

assuming standard parameters of R_m and R_i, we calculate the space constant for a foveal cone axon to be about 1000 μm (more than twice its actual length) and the space constant for a perifoveal rod axon to be greater than 500 μm. Thus, for even the longest axons simple voltage attenuation down the cable seems not to be a problem. Nor does temporal filtering seem to be an issue. The short axon of a peripheral cone at 0.5 μm diameter gives no attenuation at 20 Hz and little at 50 Hz. Therefore, there is no electrical reason that we can imagine for the short axon to be thick. The long axon of a foveal cone does attenuate temporal frequencies above 20 Hz, even though it is thick. Thus increasing axon caliber for the foveal cone does not solve this problem, and indeed we are more sensitive to high temporal frequencies in the periphery than in the fovea [60].

However, cable design for photoreceptors is rather more complicated and must take into account: (1) electrical properties of the outer segment and the terminal; (2) non-electrical functions of the cable; (3) supraordinate considerations, such as efficient use of space. Here we indicate briefly how the present analysis bears on each of these issues.

4.1. Electrical properties

The compartmental models of the cone and rod suggest no electrical reason why, for the standard (short) axon, the cone axon should be almost 4-fold thicker than the rod axon. Photovoltage generated by the cone's ohmic transducer would propagate adequately in space and time even if the axon were thin (Fig. 4A, Fig. 6). Conversely, the rod's constant current transducer is not the key to its axon being thin: an ohmic source would work equally well. But when the terminal contains an extra conductance (representing $GABA_A$ receptors), the models behave quite differently. The cone terminal leak hyperpolarizes the steady potential while hardly affecting the photovoltage (Fig. 4A vs Fig. 5B). The rod terminal leak markedly hyperpolarizes the steady potential and sharply reduces the photovoltage. The reason is that, although the rod outer segment provides constant current over a range of voltages, the voltage response declines due to an impedance mismatch.

These differences seem suited to the different integrative properties at the synapse. The cone terminal's steady hyperpolarization by a GABA-mediated Cl^- leak would be reduced by illumination of surrounding cones because they would hyperpolarize horizontal cells and shut off the GABA. Thus surround illumination would tend to depolarize the center cone without affecting the amplitude of its response to illumination. This is a plausible mechanism for the cone's antagonistic surround [61–63] which subtracts spatially redundant information [64] and thus prevents saturation by transient signals [65]. Presumably this surround antagonism is the basis for 'subtractive adaptation' observed psychophysically and assigned to the outer plexiform layer [66].

Because the rod terminal's Cl^- leak attenuates photovoltage, it is unsuitable for subtracting the background from a graded center signal. But at low light intensity the rod signal is not graded. Instead it is binary, signaling 0 or 1 photoisomerization [7,67]. This signal tends to be degraded, not by redundant signals in other rods (so psychophysical 'subtractive adaptation' is not needed; [66]) but rather by their dark noise. A leak that attenuates photovoltage would equally attenuate dark noise and thus could contribute to a thresholding mechanism, which has been postulated by previous studies [32,68,69]. This result might suggest that the 'current source' transducer and Cl^- leak are well matched for thresholding at the terminal of the mammalian rod. However, the amphibian rod, which transduces a graded signal like a cone, also behaves like a current source, so the reason for the ohmic versus current source behavior remains unclear.

4.2. A non-electrical function of the axon

If standard cable properties accounted completely for axon thickness, one would expect shorter cone axons to be thinner. However, the cone axon is thick, independent of its length, and in all species [5]. This might reflect a requirement of graded signal transmission, since the rod axon is also thick where its signal is graded (e.g. salamander) and thin where its signal is binary (mammals). Graded transmission also correlates with the number of ribbon synapses in the terminal; thus cones and salamander rods have many ribbons, but mammalian rods have only one [70,71]. In fact, the axon's cross-sectional area is directly proportional to the number of ribbons. Thus the nearly 15-fold ratio found for cone/rod axon area (Fig. 3) is paralled by their 20-fold ratio of ribbon synapses. A similar proportionality between axon cross-section and number of ribbon synapses is found for six types of bipolar axon in cat retina, all identical in length [72].

To transmit a graded signal requires a high rate of transmitter release [9,72,73]. Estimates at a variety of ribbon synapses suggest about 100 vesicles/s for an upper bound to the tonic rate [72]. Thus, a primate cone terminal would tonically release on the order of 2000 vesicles/s and the rod terminal only 100 vesicles/s [74]. Although synaptic vesicles recycle within the terminal [75], the number of cycles of fusion retrieval that a vesicle can sustain is probably limited. This implies a substantial exchange of synaptic vesicle components between soma and the terminal, a traffic conducted by kinesin motors that run on microtubule 'tracks' [76,77]. For a given motor speed, the rate of delivery depends on the number of tracks (independent of length). Therefore a higher release rate sustained by a cone terminal might well

require correspondingly more tracks and thus a thicker axon. We note in this regard that a retina-specific kinesin is most intensely expressed in photoreceptor terminals [78].

4.3. Space efficiency

The initial impetus for this study was a consideration of space; the presumed selective pressure to keep the axons of Henle's layer thin. Our calculations suggest that the long axon of a foveal cone is as thin as it can be without spatial decrement; however, a peripheral cone axon could be thinner, if cable properties were the only issue. Rods are more numerous than cones (beyond the fovea) by up to 20-fold [79,80], so the pressure to minimize cell volume must act strongly on rods. Indeed, for volume of axon + terminal the rod is reduced to about 10% of the cone. Were this volume the same as a cone's the retina's total postreceptoral thickness (from vitreal surface to the level where light is trapped at the inner segments) would roughly double.

In conclusion, it is sobering to recognize the importance of 'space efficiencies' in retinal architecture. And it is equally sobering to realize, as the present calculations suggest, how very many considerations enter the design of what at first seems like a simple wire.

Acknowledgements

We thank Stanley J. Schein for his collaboration in preparing the material, Pat Masarachia and Sally Shrom for their assistance in photographing it, Christina Geueke for preparing the figures, and Sharron Fina for preparing the manuscript. We also thank Noga Vardi, Rukmini Rao, Martin Wilson, K.-Y. Yau, and Edward Pugh for comments. Supported by EY08124 and MH48168.

References

[1] Yau K-W, Baylor DA. Cyclic GMP-activated conductance of retinal photoreceptor cells. In: Cowan WM, Shooter EM, Stevens CF, Thompson RF, editors. Annual Review Neuroscience. Palo Alto: Annual Reviews, 1989:289–327.
[2] Yau K-W. Phototransduction mechanism in retinal rods and cones. Invest Ophthalmol Vis Sci 1994;35:9–32.
[3] Wu SM. Synaptic transmission in the outer retina. Ann Rev Physiol 1994;56:141–68.
[4] Penn RD, Hagins WA. Kinetics of the photocurrent of retinal rods. Biophys J 1972;12:1073–94.
[5] Lasater EM, Normann RA, Kolb H. Signal integration at the pedicle of turtle cone photoreceptors: An anatomical and electrophysiological study. Vis. Neurosci 1989;2:553–64.
[6] Parsons TD, Lenzi D, Almers W, Roberts WM. Calcium-triggered exocytosis and endocytosis in an isolated presynaptic cell: Capacitance measurements in saccular hair cells. Neuron 1994;13(4):875–83.
[7] Rao R, Buchsbaum G, Sterling P. Rate of quantal transmitter release at the mammalian rod synapse. Biophys J 1994;67:57–63.
[8] von Gersdorff H, Matthews G. Dynamics of synaptic vesicle fusion and membrane retrieval in synaptic terminals. Nature 1994;367:735–9.
[9] de Ruyter van Steveninck R, Laughlin SB. The rate of information transfer at graded-potential synapses. Nature 1996;379:642–5.
[10] Rieke F, Schwartz EA. Asynchromous transmitter release: control of exocytosis and endocytosis at the salamander rod synapse. J Physiol 1996;493:1–8.
[11] von Gersdorff H, Vardi E, Matthews G, Sterling P. Evidence that vesicles on the synaptic ribbon of retinal bipolar neurons can be rapidly released. Neuron 1996;16:1221–7.
[12] Tsukamoto Y, Masarachia P, Schein SJ, Sterling P. Gap junctions between the pedicles of macaque foveal cones. Vis Res 1992;32:1809–15.
[13] Rall W. Core conductor theory and cable properties of neurons. In: Kandel ER, Brookhardt JM, Montcastle VB, editors. Handbook of Physiology: the Nervous System. Baltimore MD: Williams and Wilkins, 1977:39–98.
[14] Segev I, Fleshman JW, Burke RE. Compartmental models of complex neurons. In: Koch C, Segev I, editors. Methods in neuronal modeling: from synapses to networks. MIT Press: Cambridge MA, 1989:63–96.
[15] Smith RG. NeuronC: a computational language for investigating functional architecture of neural circuits. J Neurosci Methods 1992;43:83–108.
[16] Johnston D, Brown TH. Interpretation of voltage-clamp measurements in hippocampal neurons. J Neurophysiol 1983;50:464–86.
[17] Spruston N, Johnson D. Perforated patch-clamp analysis of the passive membrane properties of three classes of hippocampal neurons. J Neurophysiol 1992;67(3):508–29.
[18] Attwell D, Werblin FS, Wilson M. The properties of single cones isolated from the tiger salamander retina. J Physiol 1982;328:259–83.
[19] Jack JJB, Noble D, Tsien RW. Electric Current Flow in Excitable Cells. Oxford: Clarendon Press, 1988.
[20] Haynes L, Yau KW. Cyclic GMP-sensitive conductance in outer segment membrane of catfish cones. Nature 1985;317:61–4.
[21] Cohen AI. Further studies on the question of the patency of saccules in outer segments of vertebrate photoreceptors. Vis Res 1970;10:445–53.
[22] Rodieck RW. The Vertebrate Retina: Principles of Structure and Function. San Francisco CA: W.H.Freeman, 1973.
[23] Greeff R. @ Die Mikroskopische Anatomie des Sehnerven und der Netzhaut. Leipzig: W. Engelmann, 1899.
[24] Schnapf JL, Nunn BJ, Meister M, Baylor DA. Visual transduction in cones of the monkey Macaca fascicularis. J Physiol 1990;427:681–713.
[25] Yagi T, MacLeish PR. Ionic conductances of monkey solitary cones inner segments. J Neurophysiol 1996;71:656–65.
[26] Barnes S. After transduction: Response shaping and control of transmission by ion channels of the photoreceptor inner segment. Neurosci 1994;58:447–59.
[27] Schneeweis DM, Schnapf JL. Photovoltage of rods and cones in the macaque retina. Science 1995;268:1053–6.

[28] Koch C. Cable theory in neurons with active, linearized membranes. Biol Cybernetics 1984;50:15–33.
[29] Wu S. Input-output relations of the feedback synapse between horizontal cells and cones in the tiger salamander retina. J Neurophysiol 1991;65:1197–206.
[30] Bader CR, MacLeish PR, Schwartz EA. A voltage-clamp study of the light response in solitary rods of the tiger slamander. J Physiol 1979;296:1–26.
[31] Baylor DA, Nunn BJ. Electrical properties of the light-sensitive conductance of rods of the salamander *Ambystoma tigrinum*. J Physiol 1986;371:115–45.
[32] Baylor DA, Nunn BJ, Schnapf JL. The photocurrent, noise and spectral sensitivity of rods of the monkey Macaca fascicularis. J Physiol 1984;357:575–607.
[33] Bader CR, Bertrand D, Schwartz EA. Voltage-activated and calcium activated currents studied in solitary rod inner segments from the salamander retina. J Physiol 1982;331:253–84.
[34] Attwell D, Wilson M. Behaviour of the rod network in the tiger salamander retina mediated by membrane properties of individual rods. J Physiol 1980;309:287–315.
[35] Wu S. Synaptic transmission from rods to bipolar cells in the tiger salamander retina. Proce Nat Acad Sci USA 1985;82:3944–7.
[36] Sterling P, Smith RG, Rao R, Vardi N. Functional architecture of mammalian outer retina and bipolar cells. In: Archer S, Djamgoz MBA, Vallerga S, editors. Neurobiology and clinical aspects of the outer retina. London UK: Chapman and Hall, 1995:325–48.
[37] Vardi N, Morigiwa K. ON cone bipolar cells in rat express the metabotropic receptor mGluR6. Vis Neurosci 1997;14:789–94.
[38] Williams DR, Brainard DH, McMahon MJ, Navarro R. Double-pass and interferometric measures of the optical quality of the eye. J Opt Soc Am 1994;11:3123–35.
[39] Grünert U, Wässle H. GABA-like immunoreactivity in the monkey retina: A light and electron microscopic study. J Comp Neurol 1990;297:509–24.
[40] Vardi N, Masarachia P, Sterling P. Immunoreactivity to $GABA_A$ receptor in the outer plexiform layer of the cat retina. J Comp Neurol 1992;320:394–7.
[41] Vardi N, Sterling P. Subcellular localization of $GABA_A$ receptor on bipolar cells in macaque and human retina. Vis Res 1994;34:1235–46.
[42] Grigorenko EV, Yeh HH. Expression profiling of $GABA_A$ receptor ß-subunits in the rat retina. Vis Neurosci 1994;11:379–87.
[43] Linberg KA, Fisher SK. Ultrastructural evidence that horizontal cell axon terminals are presynaptic in the human retina. J Comp Neurol 1988;268:281–97.
[44] Leeper HF, Charlton JS. Response properties of horizontal cells and photoreceptor cells in the retina of the tree squirrel, Sciurus carolinensis. J Neurophysiol 1985;54:1157–66.
[45] Mangel SC. Analysis of the horizontal cell contribution to the receptive field surround of ganglion cells in the rabbit retina. J Physiol 1991;442:211–34.
[46] Murakami M, Shimoda Y, Nakatani K, Miyachi E, Watanabe S. GABA-mediated negative feedback from horizontal cells to cones in carp retina. Jpn J Physiol 1982;32:911–26.
[47] Tachibana M, Kaneko A. Gamma-aminobutyric acid acts at axon terminals of turtle photoreceptors: Difference in sensitivity among cell types. Proc Nat Acad Sci USA 1984;81:7961–4.
[48] Kaneko A, Tachibana M. Effects of gamma-aminobutyric acid on isolated cone photoreceptors of the turtle retina. J Physiol 1986;373:443–61.
[49] Piccolino M. The feedback synapse from horizontal cells to cone photoreceptors in the vertebrate retina. Prog Retinal Eye Res 1995;14:141–96.
[50] Bormann J, Hamill OP, Sakmann B. Mechanism of anion permeation through channels gated by glycine and gamma-aminobutryic acid in mouse cultured spinal neurones. J Physiol 1987;385:243–86.
[51] Gorrand JM, Bacin F. Use of reflecto-modulometry to study the optical quality of the inner retina. Ophthalamic Physiol Opt 1989;9:198–204.
[52] Enoch JM. Retinal receptor orientation and photoreceptor optics. In: Enoch JM, Tobey FLJ, editors. Vertebrate photoreceptor optics. Berlin: Springer-Verlag, 1981:127–68.
[53] Polyak SL. The Retina. University of Chicago Press, 1941.
[54] Boycott BB, Hopkins JM, Sperling HG. Cone connections of the horizontal cells of the rhesus monkey's retina. Proc R Soc (London) B 1987;229:345–79.
[55] Perry VH, Cowey A. The ganglion cell and cone distributions in the monkey's retina: Implications for central magnification factors. Vis Res 1985;25:1795–810.
[56] Schein S. Anatomy of Macaque fovea and spatial densities of neurons in foveal representation. J Comp Neurol 1988;269:479–505.
[57] Eliasof S, Werblin F. Characterization of the glutamate transporter in retinal cones of the tiger salamander. J Neurosci 1993;13:402–11.
[58] Arriza JL, Eliasof S, Kavanaugh MP, Amara SG. Excitatory amino acid transporter 5, a retinal glutamate transporter coupled toa chloride conductance. Proc Natl Acad Sci USA 1997;94:4155–60.
[59] Hagins WA, Penn RD, Yoshikami Y. Dark current and photocurrent in retinal rods. Biophys J 1970;10:380–412.
[60] Allen D, Hess RF. Is the vision field temporall homogenous? Vis Res 1992;32:1075–81.
[61] Baylor DA, Fuortes MG F, O'Bryan PM. Receptive fields of cones in the retina of the turtle. J Physiol 1971;214:265–94.
[62] Piccolino M, Neyton J, Gerschenfeld H. Center-surround antagonistic organization in small-field luminosity horizontal cells of turtle retina. J Neurosci 1981;45:363–75.
[63] Smith RG. Simulation of an anatomically-defined local circuit: The cone-horizontal cell network in cat retina. Vis Neurosci 1995;12:545–61.
[64] Srinivasan MV, Laughlin SB, Dubs A. Predictive coding: A fresh view of inhibition in the retina. Proc R Soc (London) B 1982;216:427–59.
[65] Burkhardt DA. The influence of center-surround antagonism on light adaptation in cones in the retina of the turtle. Vis Neurosci 1995;12:877–85.
[66] Hayhoe MM, Smith MV. The role of spatial filtering in sensitivity regulation. Vis Res 1989;29:457–69.
[67] Smith RG, Freed MA, Sterling P. Microcircuitry of the dark-adapted cat retina: functional architecture of the rod-cone network. J Neurosci 1986;6:3505–17.
[68] Freed MA, Smith RG, Sterling P. Rod bipolar array in the cat retina: pattern of input from rods and GABA-accumulating amacrine cells. J Comp Neurol 1987;266:445–55.
[69] van Rossum MCW, Smith RG. Noise removal at the rod synapse of mammalian retina. Vis Neurosci, in press.
[70] Townes-Anderson E, MacLeish PR, Raviola E. Rod cells dissociated from mature salamander retina: ultrastructure and uptake of horseradish peroxidase. J Cell Biol 1985;100:175–88.
[71] Rao-Mirotznik R, Harkins A, Buchsbaum G, Sterling P. Mammalian rod terminal: Architecture of a binary synapse. Neuron 1995;14:561–9.
[72] Rieke F, Schwartz EA. Asynchromous transmitter release:control of exocytosis and endocytosis at the salamander rod synapse. J. Physiol 1996;493:1–8.
[73] Juusola M, French AS, Uusitalo RO, Weckström M. Information processing by graded-potential transmission through tonically active synapses. Trends Neurosci 1996;19:292–7.

[74] Rao-Mirotznik R, Buchsbaum G. Sterling P. Functional architecture of the mammalian rod synapse, 1998:submitted.
[75] Schaeffer SF, Raviola E. Membrane recycling in the cone cell endings of the turtle retina. J Cell Biol 1978;79:802–25.
[76] Sheetz M, Steuer E, Schroer T. The mechanism and regulation of fast axonal transport. Trends Neurosci 1989;12:474–8.
[77] Vallee RB, Bloom GS. Mechanisms of fast and slow axonal transport. Annu Rev Neurosci 1991;14:59–92.
[78] Burnside B, Bost-Usinger LM, Hoang E. Multiple kinesin family members expressed in human retina include a potential human homologue of FKIF2, Investigative Ophthalmol Vis Sci, 1997;38: S1165 (Abstract).
[79] Packer O, Hendrickson A, Curcio C. Photoreceptor topography of the retina in the adult pigtail Macaque (*Macaca nemestrina*). J Comp Neurol 1989;288:165–83.
[80] Wikler KC, Williams RW, Rakic P. Photoreceptor mosaic: Number and distribution of rods and cones in the Rhesus monkey retina. J Comp Neurol 1990;297:499–508.